

Better Not to Propagate: Understanding Edge Uncertainty and Over-smoothing in Signed Graph Neural Networks

Yoonhyuk Choi¹, Jiho Choi², Taewook Ko³, Chong-Kwon Kim⁴

Samsung SDS¹, KAIST², Seoul National University³, Korea Institute of Energy Technology⁴
chldbsgur123@gmail.com, jihochoi@kaist.ac.kr, taewook.ko@snu.ac.kr, ckim@kentech.ac.kr

Abstract

Local smoothing, driven by message-passing (MP) under varying homophily levels, is crucial in Graph Neural Networks (GNNs). Recent research has examined this smoothing effect, which diminishes node separability after MP, by analyzing the expected distribution of node features. These studies offer theoretical insights into the local smoothing effects of different propagation methods, such as positive, signed, and blocked MPs. Node separability is theoretically determined by two hyperparameters: a fixed local homophily and a dynamic edge error ratio. However, previous analyses have constrained these values, potentially limiting optimal MP selection for GNNs. To overcome this, we propose a novel method for estimating homophily and edge error ratios, along with a dynamic selection mechanism between blocked and signed propagation during training. Our theoretical analysis with extensive experiments shows that blocking MP outperforms signed propagation under high edge error ratios, improving performance in both homophily and heterophily.

Introduction

Graph Neural Networks (GNNs) have shown remarkable performance with the aid of a message-passing (MP), where the representation of each node is recursively updated using its neighboring nodes based on structural properties (Defferrard, Bresson, and Vandergheynst 2016; Kipf and Welling 2016; Velickovic et al. 2017). Early GNNs rely on network homophily, assuming that connected nodes will likely share similar labels. However, many real-world graphs have low homophily (a.k.a. heterophilic) (Zhu et al. 2020; Ma et al. 2021; Luan et al. 2022), where spectral-based GNNs (Wang and Zhang 2022) achieve dismal performance under this condition since Laplacian smoothing only receives low-frequency signals from neighboring nodes.

To separate the embeddings of connected but dissimilar nodes, recent algorithms employ high-pass filters by adjusting edge weights during MP (Velickovic et al. 2017; Brody, Alon, and Yahav 2021; Chen et al. 2023; Liao et al. 2024). Notably, flipping the sign of edges from positive to negative known as signed propagation (Chien et al. 2020; Bo et al. 2021), or blocking MP by assigning zero weights to heterophilic connections (Luo et al. 2021; Hu et al. 2021; Tian

et al. 2022) has recently achieved remarkable performance. These techniques represent significant advancements in the field, offering new ways to enhance the performance and applicability of GNNs in diverse graph structures.

Recently, efforts have been made to theoretically analyze the effect of various propagation schemes in terms of node separability (Ma et al. 2021; Yan et al. 2021; Aseem et al. 2023) building upon the insights of the Contextual Stochastic Block Model (CSBM) (Deshpande et al. 2018). In detail, they measure the distance of node feature expectations from a decision boundary, demonstrating that signed propagation outperforms plain message-passing algorithms in binary classification tasks. More recently, (Choi et al. 2023; Li, Mei, and Ma 2024) provided new insights by extending the analysis to multiple classes and considering degree distributions. However, few efforts have been made to determine whether signed MP consistently improves separability compared to not using propagation.

In this paper, we focus on the work of (Luo et al. 2021), which mitigates local smoothing by assigning zero weights (blocking information) to heterophilic edges. Building on prior theoretical analysis, we propose the estimation of two latent parameters during training: homophily and edge classification error ratios. Based on this, we argue that MP (even with signed propagation) may result in poor performance compared to not propagating under specific conditions. Therefore, we suggest adaptively blocking information based on these values. Finally, since these values may not be easily measurable during the training phase, we propose an estimation strategy using the validation score. In summary, our contributions are as follows:

- Unlike previous methods that focused solely on signed propagation to prevent over-smoothing, we demonstrate that message passing may degrade the separability of graph neural networks under certain conditions.
- To mitigate the smoothing effect, we propose an adaptive propagation approach based on the estimated parameters. We show that blocking information can be more efficient depending on the homophily and edge error ratios.
- Extensive experiments on real-world benchmark datasets with state-of-the-art baselines show notable performance improvements, validating the proposed scheme.

Preliminaries

Notations. Let $\mathcal{G} = (\mathcal{V}, \mathcal{E}, X)$ be a graph with $|\mathcal{V}| = n$ nodes and $|\mathcal{E}| = m$ edges. The node attribute matrix is $X \in \mathbb{R}^{n \times F}$, where F is the dimension of an input vector. Given X , the hidden representation of node features H^l at the l -th layer is derived through message-passing. Here, node i 's feature is defined as h_i^l . The structural property of \mathcal{G} is represented by its adjacency matrix $A \in \{0, 1\}^{n \times n}$. A diagonal matrix with node degrees D is derived from A as $d_{ii} = \sum_{j=1}^n A_{ij}$. Each node has its label $Y \in \mathbb{R}^{n \times C}$ (C represents the number of classes).

Message-Passing (MP). Generally, GNNs employ alternate steps of propagation and aggregation recursively, during which the node features are updated iteratively. The widely known MP algorithm is GCN (Kipf and Welling 2016), which can be represented as:

$$H^{l+1} = \sigma(\tilde{A}^l H^l W^l) \quad (1)$$

Here, $H^0 = X$ is the initial vector and H^l is nodes' hidden representations at the l -th layer. H^{l+1} is retrieved through message-passing ($\tilde{A} = D^{-1}A$) with an activation function σ . W^l is trainable weight matrices. The final prediction is produced by applying cross-entropy $\sigma(\cdot)$ (e.g., log-softmax) to H^L and the loss function is defined as below:

$$\mathcal{L}_{GNN} = \mathcal{L}_{nll}(Y, \hat{Y}) \leftarrow \hat{Y} = \sigma(H^L) \quad (2)$$

The loss is computed through a negative log-likelihood \mathcal{L}_{nll} between true labels (Y) and predictions, $\hat{Y} = \sigma(H^L)$.

Homophily. \mathcal{H}_g stands for the global edge homophily ratio, which is defined as:

$$\mathcal{H}_g \equiv \frac{\sum_{(i,j) \in \mathcal{E} \mid (Y_i=Y_j)} 1}{|\mathcal{E}|} \quad (3)$$

Likewise, the local homophily ratio, b_i , of node i is given as:

$$b_i \equiv \frac{\sum_{j=1}^n A_{ij} \cdot 1(Y_i = Y_j)}{d_{ii}} \quad (4)$$

Given a partially labeled training set \mathcal{V}_L , the goal of semi-supervised node classification is to correctly predict the classes of unlabeled nodes $\mathcal{V}_U = \{\mathcal{V} - \mathcal{V}_L\} \subset \mathcal{V}$.

Over-smoothing. As introduced in (Oono and Suzuki 2019; Cai and Wang 2020), over-smoothing measures the distinguishability of node features as follows:

$$\mu(H^l) := \|H^l - 1 \frac{1^T H^l}{N}\|_F \quad (5)$$

The over-smoothing happens if $\lim_{l \rightarrow \infty} \mu(H^l) = 0$, where the node representation converges to zero after infinite propagation. Recently, (Mao et al. 2024) prove that even the attention-based GNN (Velickovic et al. 2017) loses the separability exponentially as l increases.

Motivation

We first define various MP schemes, including plain, signed, and blocking (pruning) types. Then, we introduce the prior theorems on local smoothing using the Contextual Stochastic Block Models. Finally, we highlight their drawbacks and present our new insights based on the estimated parameters.

Local Smoothing on Message-Passing Schemes

We first define the concept of three MP schemes (Baranwal, Fountoulakis, and Jagannath 2021; Yan et al. 2021; Choi et al. 2023) below.

Definition 1 (Message-Passing Schemes). *Building upon the Laplacian-based degree normalization (Kipf and Welling 2016), a.k.a. GCN, each propagation scheme modifies the adjacency matrix $\tilde{A} = D^{-1}A$ (Eq. 1) as follows:*

- **Plane MP** inherits the original matrix, which only consists of positive edges.

$$\forall (i, j) \in \mathcal{E}, \quad \tilde{A} = D^{-1}A \geq 0 \quad (6)$$

- **Signed MP** assigns negative values to the heterophilic edges, where $y_i \neq y_j$.

$$\forall (i, j) \in \mathcal{E}, \quad \tilde{A} \in \begin{cases} D^{-1}A, & y_i = y_j \\ -D^{-1}A, & y_i \neq y_j \end{cases} \quad (7)$$

- **Blocked MP** blocks the information propagation for heterophilic edges by assigning zero.

$$\forall (i, j) \in \mathcal{E}, \quad \tilde{A} \in \begin{cases} D^{-1}A, & y_i = y_j \\ 0, & y_i \neq y_j \end{cases} \quad (8)$$

To analyze the smoothing effect of each MP scheme, we inherit several useful notations defined in (Yan et al. 2021) as follows: (1) For all nodes $i = \{1, \dots, n\}$, their degrees $\{d_i\}$ and latent features $\{h_i\}$ are *i.i.d.* random variables. (2) Each class has the same population. (3) The scale of each class distribution after initial embedding is identical, $\|\mathbb{E}(h_i^{(0)}|y_i)\| = \mu$. Then, the feature distribution after a single hop propagation $\mathbb{E}(h^{(1)}|y_i)$ can be defined through a Contextual Stochastic Block Model (CSBM) as follows.

Definition 2 (CSBM under binary class scenario). *Assume a binary class $\mathbb{E}(h_i^{(0)}|y_i) \sim (\mu, \theta = \{0, \pi\})$ and node feature is sampled from Gaussian distribution (N) (Deshpande et al. 2018). If $y_i = 0$, the updated distribution $\mathbb{E}(h^{(1)}|y_i)$ is given by:*

$$\mathbb{E}(h^{(1)}|y_i) \sim N\left(\mu, \frac{1}{\sqrt{\deg(i)}}\right) \quad (9)$$

(Choi et al. 2023) extended binary CSBM (Eq. 9) to multiple (ternary) classes using additional angle ϕ as below:

$$\mathbb{E}(h_i^{(0)}|y_i) = (\mu, \phi, \theta), \quad (10)$$

where $\phi = \pi/2$ and $0 \leq \theta \leq 2\pi$. Note that the above equation satisfies the binary case's origin symmetry as $(\mu, \pi/2, 0) = -(\mu, \pi/2, \pi)$. Now, we define the impact of three MP schemes using a multi-class CSBM below.

Lemma 3 (Multi-class CSBM, Plane MP). *Given $y_i = 0$, let us assume ego $k \sim (\mu, \pi/2, 0)$ and aggregated neighbors $k' \sim (\mu, \pi/2, \theta')$. By replacing the $\mathbb{E}_p(h_i^{(1)}|y_i, d_i)$ as $\mathbb{E}_p(\cdot)$, the expectation after plane MP is as follows:*

$$\mathbb{E}_p(\cdot) = \frac{\{kb_i + k'(1 - b_i)\}d_i' + k}{d_i + 1} \quad (11)$$

The k' always satisfies $\|k'\| \leq \|k\|$ regardless of the normalized degree and homophily ratio since $1 - b_i \leq 1$.

Lemma 4 (Multi-class CSBM, Signed MP). *Similar to above, the expectation $\mathbb{E}_s(\cdot)$ after signed MP is given by:*

$$\mathbb{E}_s(\cdot) = \frac{(1 - 2e)\{b_i k + (b_i - 1)k'\}d'_i + k}{d_i + 1} \quad (12)$$

Remark. The notation e stands for the error ratio of incorrectly changing the sign of edges, which will be addressed throughout this paper. As introduced in (Choi et al. 2023), the sign inconsistency caused by multi-hop propagation can be solved through jumping knowledge (Xu et al. 2018).

Lemma 5 (Multi-class CSBM, Blocked MP). *Lastly, the expectation $\mathbb{E}_b(\cdot)$ driven by blocked MP can be defined as:*

$$\mathbb{E}_b(\cdot) = \frac{\{(1 - e)b_i k + e(1 - b_i)k'\}d'_i + k}{d_i + 1} \quad (13)$$

Proof of Lemma 3 - 5 are in Appendix A.

Necessity of Blocked MP

Based on the analyses above, we derive new insights into the smoothing effect of each propagation scheme. Following (Yan et al. 2021), we assume that node separability (discriminative power) is proportional to the coefficient of $\mathbb{E}_p(\cdot)$, $\mathbb{E}_s(\cdot)$, $\mathbb{E}_b(\cdot)$ in the above lemma. Through this assumption, we first show that plain MP has lower separability than signed and blocked MPs.

Corollary 6 (Plane vs Other MPs). *Since $d'_i/(d_i + 1)$ is shared for all MPs (Eq. 11 - 13), we can compare the separability by omitting them as follows:*

- (Plane vs Signed MP) By comparing Eq. 11 and 12:

$$Z_1 = \mathbb{E}_p(\cdot) - \mathbb{E}_s(\cdot) = (2e - 1)\{b_i k + (b_i - 1)k'\} \quad (14)$$

- (Plane vs Blocked MP) By comparing Eq. 11 and 13:

$$Z_2 = \mathbb{E}_p(\cdot) - \mathbb{E}_b(\cdot) = eb_i k + (1 - e)(1 - b_i)k' \quad (15)$$

The $\iint_{e, b_i} Z_1$ and $\iint_{e, b_i} Z_2$ are always negative, regardless of the variables b_i and e , indicating that **plain MP has the lowest discrimination power among the three MPs**. Therefore, we can focus on the separability of the signed and blocked MPs to determine the optimal propagation scheme.

Corollary 7 (Signed vs Blocked MP). *The difference between signed and blocked MP is given by:*

$$Z_3 = \mathbb{E}_s(\cdot) - \mathbb{E}_b(\cdot) = (1 - 2e)k + (b_i - e)k' \quad (16)$$

Previous studies assume a perfect edge classification scenario ($e = 0$), leading to the conclusion that $Z = 1 - b_i \geq 0$, where signed MP outperforms blocked MP. However, achieving this optimal condition is challenging in a semi-supervised setting with few training nodes. Therefore, we propose estimating two parameters, e and b_i , to select the most precise MP schemes. To facilitate understanding, we provide an example by varying e below.

Corollary 8 (Numerical example on edge error ratio). *We assume three different edge error ratios, $e = 1, 0.5, 0$ to*

compare the signed and blocked MPs. Assuming that the neighbors are i.i.d. ($k' = -k$), Eq. 16 simplifies to:

$$Z_3 = (1 - e - b_i)k = \begin{cases} -b_i k, & e = 1 \\ (-b_i + 0.5)k, & e = 0.5 \\ (1 - b_i)k, & e = 0 \end{cases} \quad (17)$$

We can infer some useful insights from the above Corollary: (1) Under a high error ratio ($e = 1$, initial stage of training), it might be better to *not propagate* rather than using signed edges since $-b_i k \leq 0$ ($Z_3 \leq 0$). In addition, an error in signed propagation increases the uncertainty more than blocked GNNs as shown in Lemma 9. (2) If the error is mediocre ($e = 0.5$), the sign of Z_3 is dependent on the homophily ratio b_i . In this condition, signed MP may perform well ($Z_3 \geq 0$) under heterophily ($b < 0.5$), but it is still advantageous not to propagate messages under homophily. (3) However, if the edges are perfectly classified ($e = 0$), signed MP might be the best option ($1 - b_i \geq 0$), as demonstrated in prior work (Choi et al. 2023). Therefore, we suggest the estimation of these two parameters, b_i and e for precise training. In addition, the following theorem reveals the necessity of blocked MP under high e in terms of uncertainty.

Theorem 9 (Uncertainty). *Under large values of e , signed MP exhibits higher entropy than the blocked ones.*

Proof can be found in Appendix B.

Methodology

Selecting an appropriate MP scheme is crucial for reducing smoothing and uncertainty. However, this may not be tractable in a semi-supervised learning context. Thus, we employ an EM algorithm, where the **E-step** is used for parameter estimation, and the **M-step** is used for optimization.

(E-Step) Parameter Estimation

We start with the strategy of homophily (b_i) and edge error (e_t) estimation in Theorem 10 and 11, respectively.

Theorem 10 (Homophily estimation). *The homophily ratio b_i can be inferred using the mechanism of MLP (Wang et al. 2022) and EvenNet (Lei et al. 2022) as follows:*

$$b_i = B_i B_i^T, \quad B := \sigma \left(\sum_{l=0}^L XW^l + \sum_{l=0}^{\lfloor L/2 \rfloor} \tilde{A}^{2l} XW^l \right) \quad (18)$$

which can take advantage of both the heterophily robustness of MLP and the low variance of EvenNet.

The proof is provided in Appendix C.

Theorem 11 (Edge error estimation). *Given the node classification accuracy of validation sets (α_{t-1}) at iteration $t-1$ and the number of classes (c), e_t can be inferred as below:*

$$e_t = 1 - \left\{ a_{t-1}^2 + \frac{(1 - a_{t-1})^2}{c - 1} \right\} \quad (19)$$

Approximation error. *Given the experimental settings in (Kipf and Welling 2016), the number of validation sets satisfies $n_{val} = 1,080 > 30$ for Cora as in Table 1. Thus, it can*

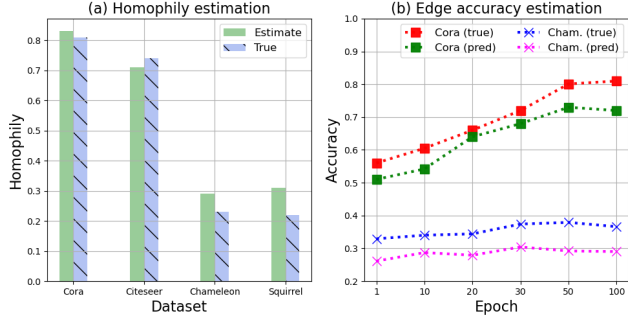


Figure 1: Empirical analysis on (a) homophily and (b) edge error estimation. More details can be found in Appendix D

be easily inferred that the feature distribution of randomly sampled validation sets ($\mathbb{E}[h_{val}]$) follows the total distribution ($\mathbb{E}[h]$) as below.

$$Z = \frac{\mathbb{E}[h_{val}] - \mathbb{E}[h]}{\text{var}(h_{val})/\sqrt{n_{val}}} \sim N(0, 1) \quad (20)$$

Now, we demonstrate that the validation samples are less likely to be biased using the concentration theorem. Given that the output of the GNN (h_i) follows a Dirichlet distribution, $\text{Dir}(h; c) = \frac{1}{B(c_1, \dots, c_K)} \prod_{k=1}^K h_i^{c_k-1}$, and assuming the classes are i.i.d., we can derive the following inequality:

$$\mathbb{P}(\|h_{val} - \mathbb{E}[h_{val}]\|_2 \geq \varepsilon) \leq 2 \cdot \exp(-2\varepsilon^2 n_{val}) \quad (21)$$

which means that the validation nodes are equally distributed around its center $\mathbb{E}[h_{val}]$.

The derivation of Eq. 19 is provided in Appendix E.

Empirical analysis. In Figure 1, we conduct empirical analyses to verify Theorem 10 (left) and 11 (right). In the figure (a), we illustrate the estimated and true homophily ratios under semi-supervised settings (Kipf and Welling 2016). In the figure (b), we compare the true and estimated edge errors (Eq. 19) for two graphs, Cora (homophilic) and Chameleon (heterophilic), during the training epochs (x-axis). As shown in both figures, the predicted values are very similar to the actual values, with minor differences likely due to the node distribution of the benchmark graph not being i.i.d. condition. Detailed experimental settings and additional results can be found in Appendix F, where the estimated values are almost identical if classes are identically distributed.

(M-Step) Optimization with Calibration

Referring to the separability of signed and blocked MP in Eq. 17, we can determine the propagation type based on the estimated values of b_i (Eq. 18) and e (Eq. 19). For each training step t , the discrimination gap between signed and blocked MP can be defined below:

$$Z_t = (1 - b_i - e_t)k \quad (22)$$

If $Z_t < 0$, we block signed messages to reduce the smoothing effect (Corollary 7) and uncertainty (Lemma 9). For a numerical definition, let us assume the adjacency matrix derived from the downstream task as \tilde{A} as defined from Eq.

Algorithm 1: Pseudo-code of our method

Input: Adjacency matrix (\tilde{A}), node features (X), initialized parameters (θ), initialized validation ($\alpha_0 = 0$) and best validation score ($\alpha^* = 0$)

Output: Parameters with the best validation score (θ^*)

- 1: Homophily estimation b_i (Eq. 18)
- 2: **for** training epochs $t \geq 1$ **do**
- 3: **(E-Step)**
- 4: Get validation score a_{t-1}
- 5: Edge error estimation e_t (Eq. 19)
- 6: **(M-Step)**
- 7: For all edges in \tilde{A}
- 8: **if** $\tilde{A}_{ij} < 0 \wedge Z_t = 1 - b_i - e_t < 0$ **then**
- 9: $\hat{A}_{ij} = 0$
- 10: **else**
- 11: $\hat{A}_{ij} = \tilde{A}_{ij}$
- 12: Message-passing, $H^{(l+1)} = \sigma(\hat{A}H^{(l)}W^{(l)})$
- 13: Node classification, $\mathcal{L}_{GNN} = \mathcal{L}_{nll}(Y, \sigma(H^{(L)}))$
- 14: Parameter update, $\theta^{(t+1)} = \theta^t - \eta \partial \mathcal{L}_{GNN} / \partial \theta^t$
- 15: Get validation score α_t
- 16: **if** $\alpha_t > \alpha^*$ **then**
- 17: Save current parameters as best, $\theta^* = \theta^t$
- 18: Update best validation score, $\alpha^* = \alpha_t$

6 to 8. Then, we calibrate the edges based on the following conditions:

$$\hat{A}_{ij} = \begin{cases} 0, & \tilde{A}_{ij} < 0 \wedge Z_t < 0 \\ \tilde{A}_{ij}, & \text{otherwise} \end{cases} \quad (23)$$

We replace the normalized adjacency matrix (\tilde{A}) in Eq. 1 with \hat{A} as follows:

$$H^{(l+1)} = \sigma(\hat{A}H^{(l)}W^{(l)}) \quad (24)$$

Then, we employ Eq. 2 (\mathcal{L}_{GNN}) for optimization, where the above strategy can be applied to general signed MPs.

Theoretical Justification

We aim to show that the proposed method can relieve the smoothing effect of signed MP using the notion of spectral radius (Def. 12 to Thm. 16) and separability (Thm. 17).

Definition 12 (Spectral Radius). *Let $\lambda_1, \dots, \lambda_n$ be the eigenvalues of an adjacency matrix $A \in \mathcal{R}^{n \times n}$. Then, the spectral radius of A is given by:*

$$\rho(A) = \max\{|\lambda_1|, \dots, |\lambda_n|\} \quad (25)$$

A^∞ is well known to converge if $\rho(A) < 1$ or $\rho(A) = 1$, where $\lambda_1 = 1$ is the only eigenvalue on the unit circle.

Definition 13 (Joint Spectral Radius). *The generalization of a spectral radius from a single matrix to a finite set of matrices $\mathcal{M} = \{A_1, \dots, A_n\}$:*

$$J_\rho(A) = \lim_{k \rightarrow \infty} \max\{\|A_1 \cdots A_k\|^{1/k} : A \in \mathcal{M}\} \quad (26)$$

where the over-smoothing occurs at an exponential rate if and only if $J_\rho(A) < 1$. In the following lemma, we first demonstrate that even attention-based MP cannot resolve the over-smoothing issue.

Lemma 14 (Attention is susceptible to over-smoothing). *For all layers l , the attention matrix \tilde{A}^l cannot change the connectivity of the original graph (Brody, Alon, and Yahav 2021) as follows:*

$$0 < \tilde{A}_{ij}^l \leq 1, \quad \forall (i, j) \in \mathcal{E} \quad (27)$$

It is well known that the infinite products of non-homogeneous row-stochastic matrices $\prod_{l=1}^{\infty} \tilde{A}^l$ converge to the same vector (Cowles and Carlin 1996; Seneta 2006), where we can easily infer that the stacking the infinite softmax-based attention matrix also converges (irreducible). Recent work (Wu et al. 2024) provided a tighter bound that GAT satisfies $J_\rho(A) < 1$ (Eq. 26), which means that $\lim_{l \rightarrow \infty} \tilde{A}^l$ converges at an exponential rate.

Unlike an attention-based matrix, where the total sum of the edge weights connected to a neighbor node is 1, a signed adjacency matrix (Eq. 7) is sub-stochastic since the sum of rows is less than 1. Therefore, the spectral radius of the sub-stochastic matrix satisfies the following conditions.

Corollary 15 (Convergence of signed MP). *Let us assume that signed MP makes the original adjacency matrix A as an irreducible sub-stochastic matrix \bar{A} (Eq. 7). Before the proof, note that the corresponding eigenvector of $\rho(\bar{A})$ satisfies $\|\lambda\|_1 = 1$ and $\epsilon_i = 1 - \sum_{j=1}^N A_{ij}$. Referring to Eq. 25, the spectral radius of the sub-stochastic matrix satisfies the condition $\rho(\bar{A}) < 1$ as below:*

$$\rho(\bar{A}) = \underbrace{\sum_{i=1}^N \sum_{j=1}^N \lambda_i (A_{ij} + \epsilon_{ij})}_{\text{stochastic matrix, } \rho(A)=1} - \underbrace{\sum_{i=1}^N \sum_{j=1}^N \epsilon_{ij}}_{>0} < 1 \quad (28)$$

which means signed MP also converges. However, our edge calibration can mitigate the smoothing effect as follows.

Theorem 16 (Edge calibration reduces local smoothing). *Based on Corollary 15, we can infer that a matrix with k -disconnected sub-stochastic components satisfies $|\lambda_1| = |\lambda_2| = \dots = |\lambda_k| = 1$. According to Definition 12, $J_\rho(\bar{A}) = 1$ with multiple λ 's on the unit circle does not meet the convergence property compared to the graph attention as in Lemma 14, relieving the smoothing effect in Eq. 5.*

Lastly, we prove that edge calibration also enhances the separability of signed MP as follows.

Theorem 17 (Separability). *Signed MP with edge calibration outperforms the original signed and blocked MPs.*

- (High $e_t \geq 0.5$, Ours (blocked) vs Signed MPs)

$$Z_4 = \mathbb{E}_b(\cdot) - \mathbb{E}_s(\cdot) = \int_{b=0}^1 \int_{e_t=0.5}^1 (1 - b_i - e_t + 2e_t b_i) = \frac{9}{8} \quad (29)$$

- (Low $e_t < 0.5$, Ours (signed) vs Blocked MPs)

$$Z_5 = \mathbb{E}_s(\cdot) - \mathbb{E}_b(\cdot) = \int_{b=0}^1 \int_{e_t=0}^{0.5} (1 - e_t - b_i) = \frac{1}{8} \quad (30)$$

Both equations satisfy $\iint_{e, b_i} Z_4 > 0$ and $\iint_{e, b_i} Z_5 > 0$, indicating that edge calibration leverages the advantages of both signed and blocked MPs under each condition.

Table 1: Details of the six benchmark graphs. We follow the experimental settings of GCN (Kipf and Welling 2016)

Datasets	Cora	Citeseer	Pubmed	Actor	Cham.	Squirrel
# Nodes	2,708	3,327	19,717	7,600	2,277	5,201
# Edges	10,558	9,104	88,648	25,944	33,824	211,872
# Features	1,433	3,703	500	931	2,325	2,089
# Labels	7	6	3	5	5	5
# Training	140	120	60	100	100	100
# Validation	1,083	1,330	7,886	3,040	910	2,080

Experiments

We conduct extensive experiments to answer the following research questions:

- **Q1:** Does the proposed method improve the node classification accuracy of signed GNNs?
- **Q2:** Does edge calibration enhance the inter-class separability of signed propagation?
- **Q3:** How does performance change given the values Z_t in Eq. 22?
- **Q4:** How much does the method improve the quality of GNNs on large benchmark graphs?

Baselines. For the experiment, we classified the baselines into two main categories: signed GNNs and others. As shown in Table 2, we applied our method to the following three signed propagation techniques for evaluation: GPRGNN (Chien et al. 2020), FAGCN (Bo et al. 2021), and GGCN (Yan et al. 2021).

Please refer to Appendix G for the details of datasets, baselines, and implementations

Performance Analysis (Q1)

Table 2 shows the node classification accuracy (%) of several state-of-the-art methods. We analyze the results from the two perspectives below.

Signed and blocked MPs Outperform Plane MP: The experimental results demonstrate that GNNs with signed or blocked MP outperform traditional methods under benchmark graphs. For both homophilic and heterophilic datasets, we can see that plane MP-based algorithms like GCN, GAT, and APPNP show inferior accuracy than others. Especially, the performance gap increases as the homophily decreases. Specifically, on the Actor dataset, GloGNN relatively outperforms GCN by over 30%. In addition, under Chameleon and Squirrel with many cyclic edges, Auto-HeG, signed (GPRGNN, FAGCN, and GGCN) or blocked (PTD-Net) MPs achieve state-of-the-art performance. This highlights the efficacy of signed and blocked GNNs in capturing the complex relationships present in general graphs, thereby leading to superior improvement.

Edge Weight Calibration Enhances the Performance of Signed GNNs: The results underscore the critical importance of edge weight calibration in enhancing the performance of signed GNNs. Models that incorporate edge weight adjustments, such as GPRGNN* and FAGCN*, consistently outperform their counterparts across a wide range of datasets, highlighting the robustness of this approach.

Table 2: (Q1) Node classification performance (%) with standard deviation (\pm) on the six benchmark graphs. The gray-colored cells indicate top-3 performance. A symbol * means that edge calibration (Eq. 23) is applied on a base method

Datasets \mathcal{H}_g (Eq. 3)	Cora	Citeseer	Pubmed	Actor	Chameleon	Squirrel
GCN (Kipf and Welling 2016)	80.5 \pm 0.73	70.4 \pm 0.62	78.6 \pm 0.44	20.2 \pm 0.40	49.3 \pm 0.58	30.7 \pm 0.70
GAT (Velickovic et al. 2017)	81.2 \pm 0.51	71.3 \pm 0.75	79.0 \pm 0.45	22.5 \pm 0.36	48.8 \pm 0.83	30.8 \pm 0.94
APPNP (Gasteiger et al. 2018)	81.8 \pm 0.51	71.9 \pm 0.38	79.0 \pm 0.30	23.8 \pm 0.32	48.0 \pm 0.77	30.4 \pm 0.61
GCNII (Chen et al. 2020)	81.3 \pm 0.69	70.7 \pm 1.28	78.5 \pm 0.50	25.9 \pm 1.21	48.6 \pm 0.76	30.4 \pm 0.90
H ₂ GCN (Zhu et al. 2020)	79.4 \pm 0.45	71.2 \pm 0.79	78.1 \pm 0.31	25.6 \pm 1.15	47.5 \pm 0.82	31.0 \pm 0.74
PTDNet (Luo et al. 2021)	81.1 \pm 0.79	71.4 \pm 1.12	78.8 \pm 0.67	21.5 \pm 0.75	50.4 \pm 1.06	32.2 \pm 0.75
P-reg (Yang, Ma, and Cheng 2021)	81.0 \pm 0.88	71.9 \pm 0.81	78.5 \pm 0.42	21.2 \pm 0.52	50.6 \pm 0.37	33.1 \pm 0.40
ACM-GCN (Luan et al. 2022)	81.6 \pm 0.85	71.3 \pm 1.01	78.4 \pm 0.53	24.9 \pm 2.17	49.6 \pm 0.59	31.2 \pm 0.44
HOG-GCN (Wang et al. 2022)	81.7 \pm 0.41	72.2 \pm 0.67	79.0 \pm 0.24	21.3 \pm 0.56	47.9 \pm 0.45	30.2 \pm 0.50
JacobiConv (Wang and Zhang 2022)	81.9 \pm 0.69	72.0 \pm 0.75	78.7 \pm 0.42	26.0 \pm 1.04	51.6 \pm 1.10	32.1 \pm 0.73
GloGNN (Li et al. 2022)	82.0 \pm 0.40	71.8 \pm 0.52	79.4 \pm 0.28	26.6 \pm 0.71	48.3 \pm 0.39	30.8 \pm 0.80
AERO-GNN (Lee et al. 2023)	81.6 \pm 0.54	71.1 \pm 0.62	79.1 \pm 0.47	25.5 \pm 1.08	49.8 \pm 2.33	29.9 \pm 1.96
Auto-HeG (Zheng et al. 2023)	81.5 \pm 1.06	70.9 \pm 1.41	79.2 \pm 0.24	26.1 \pm 0.98	48.7 \pm 1.37	31.5 \pm 1.11
TED-GCN (Yan et al. 2024)	81.8 \pm 0.88	71.4 \pm 0.56	78.6 \pm 0.30	26.0 \pm 0.95	50.4 \pm 1.21	33.0 \pm 0.98
PCNet (Li, Pan, and Kang 2024)	81.5 \pm 0.76	71.2 \pm 1.20	78.8 \pm 0.26	26.4 \pm 0.85	48.1 \pm 1.69	31.4 \pm 0.56
GPRGNN (Chien et al. 2020)	81.1 \pm 0.56	71.0 \pm 0.83	78.7 \pm 0.55	24.8 \pm 0.87	50.2 \pm 0.79	30.2 \pm 0.62
GPRGNN*	82.5 \pm 0.37	72.4 \pm 0.66	79.3 \pm 0.35	26.9 \pm 0.74	52.5 \pm 0.54	32.2 \pm 0.49
Relative improv. (+ %)	+ 1.73 %	+ 1.97 %	+ 0.76 %	+ 8.47 %	+ 4.58 %	+ 6.62 %
FAGCN (Bo et al. 2021)	81.4 \pm 0.51	72.2 \pm 0.69	78.9 \pm 0.62	25.3 \pm 0.77	49.1 \pm 1.20	30.3 \pm 0.96
FAGCN*	82.8 \pm 0.45	73.4 \pm 0.50	79.6 \pm 0.33	27.8 \pm 0.58	51.8 \pm 0.91	32.5 \pm 0.77
Relative improv. (+ %)	+ 1.72 %	+ 1.66 %	+ 0.89 %	+ 9.88 %	+ 5.50 %	+ 7.26 %
GGCN (Yan et al. 2021)	81.2 \pm 1.06	71.5 \pm 1.44	78.3 \pm 0.35	23.7 \pm 0.75	50.0 \pm 0.98	30.4 \pm 0.72
GGCN*	82.4 \pm 0.87	73.0 \pm 0.72	79.0 \pm 0.34	25.6 \pm 0.61	52.0 \pm 0.72	32.7 \pm 0.69
Relative improv. (+ %)	+ 1.48 %	+ 2.10 %	+ 0.89 %	+ 8.02 %	+ 4.00 %	+ 7.57 %

For instance, GPRGNN* demonstrates remarkable performance improvements on both the Cora and Pubmed datasets compared to the baseline GPRGNN, indicating its adaptability and effectiveness. Similarly, FAGCN*, including edge weight calibration, outperforms the original FAGCN model on homophilic and heterophilic graphs, showcasing its versatility in different graph structures. Additionally, our method leverages blocked MP by effectively removing cyclic edges for the Chameleon and Squirrel datasets, further enhancing model performance. These findings collectively suggest that edge weight calibration is crucial for maximizing the full potential of signed GNNs, as it plays a pivotal role in reducing the smoothing effect under edge uncertainty and ultimately achieving higher classification accuracy across diverse scenarios.

Analysis on Discrimination Power (Q2)

In Figure 2, we present the inter-class distances for three GNNs with signed MP (GPRGNN, FAGCN, and GGCN) across four benchmark graphs (Cora, Citeseer, Actor, and Squirrel) to investigate a neural collapse perspective (Kothapalli, Tirer, and Bruna 2024). The y-axis measures the average L2 distance between classes after the first layer projection. To ensure fairness, we removed parameter randomness from all baselines. The ensemble methods (indicated with an asterisk) consistently show an increase in inter-class distance compared to their standard counterparts across all datasets. For instance, on the Cora dataset, GPRGNN* and FAGCN* show increases to 1.06 and 1.43, respectively,

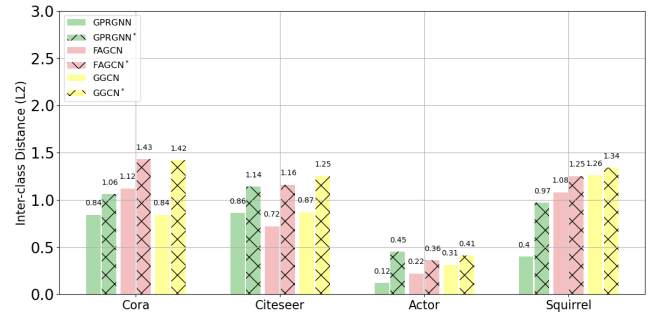


Figure 2: (Q2) We take three signed GNNs (GPRGNN, FAGCN, and GGCN) and measure the inter-class distances to show that our method improves the discrimination power

compared to 0.84 and 1.12 for the standard models. The increase is even more substantial in heterophilic datasets like Actor and Squirrel, where the methods with edge calibration significantly improve separability compared to the standard versions, highlighting the effectiveness of blocked MP under certain conditions.

Importance of Proper MP Schemes (Q3)

We aim to show that selecting a proper propagation scheme between signed or blocked MPs is crucial for GNNs. As described in Figure 3, the x-axis stands for the Z_t in Eq. 22, and the y-axis represents node classification accuracy. For a

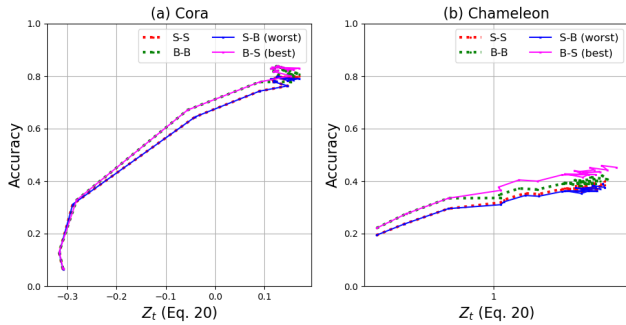


Figure 3: (Q3) Performance gain concerning signed/blocked propagation using FAGCN* model

fair comparison, we remove the randomness for all methods (e.g., parameter initialization) by fixing the seed. The left figure is (a) Cora and the right one is (b) Chameleon. We have proved that blocked MP outperforms signed MP in the case of $Z_t < 0$, and vice versa. To verify this, we assume two types of MPs: signed (S) and blocked (B) under two different conditions: $Z_t < 0$ and $Z_t \geq 0$. For example, S-S means that signed MPs are used independent of Z_t , while B-S utilizes blocked MP if $Z_t < 0$ and signed MP for $Z_t \geq 0$. As illustrated, selecting the proper propagation scheme (B-S) achieves the best quality, where the performance gap becomes greater in the heterophilic graph (Chameleon). Conversely, improper MPs (S-B or S-S) when $Z_t < 0$ show low accuracy, showing that blocked MP can improve the quality of prediction under this condition significantly.

Table 3: (Q4) Node classification accuracy (%) on large heterophilic graphs. Penn94 has a binary class, while the arXiv-year and snap-patents have five classes

Datasets	Penn94	arXiv-year	snap-patents
\mathcal{H}_g (Eq. 3)	0.046	0.272	0.1
GCN (Kipf and Welling 2016)	81.3 \pm 0.3	44.5 \pm 0.3	43.9 \pm 0.2
GAT (Velickovic et al. 2017)	80.6 \pm 0.6	45.0 \pm 0.5	45.2 \pm 0.6
GCNII (Chen et al. 2020)	81.8 \pm 0.7	46.1 \pm 0.3	47.5 \pm 0.7
H ₂ GCN (Zhu et al. 2020)	80.4 \pm 0.6	47.6 \pm 0.2	OOM
GPRGNN (Chien et al. 2020)	80.9 \pm 0.3	43.6 \pm 0.4	41.4 \pm 0.1
GPRGNN*	83.1 \pm 0.4	44.9 \pm 0.3	43.6 \pm 0.3
Relative improv. (+ %)	2.72%	2.98%	5.3%

Analysis on Large Graphs (Q4)

We conduct experiments on large benchmarks (Lim et al. 2021) and describe the results in Table 3. Due to the OOM issue, we apply our method to one of the memory-efficient signed GNNs, GPRGNN (Chien et al. 2020). As shown in the table, our method GPRGNN* demonstrates notable improvements in node classification accuracy across large graphs. Specifically, on the three datasets, GPRGNN* achieves an accuracy improvement of 2.72%, 2.98%, and 5.3% over the baseline GPRGNN, respectively. Although H₂GCN (Zhu et al. 2020) and GCNII (Chen et al. 2020) show the best performance on arXiv and snap, this is because the accuracy of the original GPRGNN is quite lower

compared to the other methods. To summarize, these results highlight the effectiveness of our approach in enhancing the performance of GNNs on large-scale benchmarks.

Related Work

Heterophilic GNNs. Starting from Laplacian decomposition (Defferrard, Bresson, and Vandergheynst 2016), spectral GNNs (Kipf and Welling 2016; Wang and Zhang 2022; Du et al. 2022; Bo et al. 2023; Lu et al. 2024) have achieved remarkable performance on homophilic graphs. However, as the homophily (Platonov et al. 2024) of the graph decreases, their performance sharply declines due to local smoothing (Pei et al. 2020). To address this limitation, spatial-based GNNs have emerged, developing many powerful schemes that adjust edge weights for message-passing (Velickovic et al. 2017; Brody, Alon, and Yahav 2021; Chen et al. 2023; Liao et al. 2024). Specifically, some studies handle disassortative edges by capturing node differences or incorporating similar remote nodes as neighbors (Derr, Ma, and Tang 2018; Huang et al. 2019; Zhu et al. 2020; Choi et al. 2022; Lei et al. 2022; Wang et al. 2022; Zhao et al. 2023; Zheng et al. 2023; Mao et al. 2024; Yan et al. 2024; Li, Pan, and Kang 2024; Qiu et al. 2024; Tang et al. 2024). Among these, methods that either change the sign of the edge (Chien et al. 2020; Bo et al. 2021; Fang et al. 2022; Guo and Wei 2022) or opt not to transmit information (Luo et al. 2021; Hu et al. 2021; Tian et al. 2022) have recently been proposed.

Over-smoothing in GNNs. In addition to the above methods, theoretical analyses have emerged explaining why each message-passing technique works well from the perspective of node separability (reduced smoothing effect). For example, (Yan et al. 2021; Baranwal, Fountoulakis, and Jagannath 2021) analyzed the separability of the plane, signed, and blocked propagation after message-passing under binary class graphs. Recently, (Choi et al. 2023) extended the theorems to multi-class scenarios, and (Li, Mei, and Ma 2024) suggested their degree-corrected version. However, these methods assume a fixed edge classification error, which may fail to induce the smoothing effect precisely.

Conclusion

This paper presents a comprehensive study on the impact of edge uncertainty and over-smoothing in signed Graph Neural Networks (GNNs). First, we scrutinize the smoothing effect under different values of Z_t (Eq. 22), offering a novel perspective that propagation schemes should account for varying homophily and edge classification error ratios. Second, we introduce an innovative training mechanism that dynamically selects between blocked and signed propagation based on these parameters, effectively mitigating over-smoothing and enhancing performance. Our theoretical analysis, supported by extensive experiments, demonstrates that blocking message propagation can be more effective than traditional message-passing schemes under certain conditions. This insight is crucial for improving node classification accuracy in both homophilic and heterophilic graphs. We hope that future work will explore further refinements of these techniques for more complex graph structures.

References

- Aseem, B.; Kimon, F.; Aukosh, J.; and et, a. 2023. Effects of Graph Convolutions in Multi-layer Networks. In *The Eleventh International Conference on Learning Representations*.
- Baranwal, A.; Fountoulakis, K.; and Jagannath, A. 2021. Graph convolution for semi-supervised classification: Improved linear separability and out-of-distribution generalization. *arXiv preprint arXiv:2102.06966*.
- Bo, D.; Shi, C.; Wang, L.; and Liao, R. 2023. Specformer: Spectral graph neural networks meet transformers. *arXiv preprint arXiv:2303.01028*.
- Bo, D.; Wang, X.; Shi, C.; and Shen, H. 2021. Beyond low-frequency information in graph convolutional networks. *arXiv preprint arXiv:2101.00797*.
- Brody, S.; Alon, U.; and Yahav, E. 2021. How attentive are graph attention networks? *arXiv preprint arXiv:2105.14491*.
- Cai, C.; and Wang, Y. 2020. A note on over-smoothing for graph neural networks. *arXiv preprint arXiv:2006.13318*.
- Chen, M.; Wei, Z.; Huang, Z.; Ding, B.; and Li, Y. 2020. Simple and deep graph convolutional networks. In *International Conference on Machine Learning*, 1725–1735. PMLR.
- Chen, Y.; Luo, Y.; Tang, J.; Yang, L.; Qiu, S.; Wang, C.; and Cao, X. 2023. LSGNN: Towards General Graph Neural Network in Node Classification by Local Similarity. *arXiv preprint arXiv:2305.04225*.
- Chien, E.; Peng, J.; Li, P.; and Milenkovic, O. 2020. Adaptive universal generalized pagerank graph neural network. *arXiv preprint arXiv:2006.07988*.
- Choi, Y.; Choi, J.; Ko, T.; Byun, H.; and Kim, C.-K. 2022. Finding Heterophilic Neighbors via Confidence-based Subgraph Matching for Semi-supervised Node Classification. In *Proceedings of the 31st ACM International Conference on Information & Knowledge Management*, 283–292.
- Choi, Y.; Choi, J.; Ko, T.; and Kim, C.-K. 2023. Is signed message essential for graph neural networks. *arXiv preprint arXiv:2301.08918*.
- Cowles, M. K.; and Carlin, B. P. 1996. Markov chain Monte Carlo convergence diagnostics: a comparative review. *Journal of the American statistical Association*, 91(434): 883–904.
- Defferrard, M.; Bresson, X.; and Vandergheynst, P. 2016. Convolutional neural networks on graphs with fast localized spectral filtering. *Advances in neural information processing systems*, 29.
- Derr, T.; Ma, Y.; and Tang, J. 2018. Signed graph convolutional networks. In *2018 IEEE International Conference on Data Mining (ICDM)*, 929–934. IEEE.
- Deshpande, Y.; Sen, S.; Montanari, A.; and Mossel, E. 2018. Contextual stochastic block models. *Advances in Neural Information Processing Systems*, 31.
- Du, L.; Shi, X.; Fu, Q.; Ma, X.; Liu, H.; Han, S.; and Zhang, D. 2022. Gbk-gnn: Gated bi-kernel graph neural networks for modeling both homophily and heterophily. In *Proceedings of the ACM Web Conference 2022*, 1550–1558.
- Fang, Z.; Xu, L.; Song, G.; Long, Q.; and Zhang, Y. 2022. Polarized Graph Neural Networks. In *Proceedings of the ACM Web Conference 2022*, 1404–1413.
- Gasteiger, J.; Bojchevski, A.; Gunnemann, S.; and Johns. 2018. Predict then propagate: Graph neural networks meet personalized pagerank. *arXiv preprint arXiv:1810.05997*.
- Guo, Y.; and Wei, Z. 2022. Clenshaw Graph Neural Networks. *arXiv preprint arXiv:2210.16508*.
- Hu, Y.; You, H.; Wang, Z.; Wang, Z.; Zhou, E.; and Gao, Y. 2021. Graph-mlp: Node classification without message passing in graph. *arXiv preprint arXiv:2106.04051*.
- Huang, J.; Shen, H.; Hou, L.; and Cheng, X. 2019. Signed graph attention networks. In *International Conference on Artificial Neural Networks*, 566–577. Springer.
- Kipf, T. N.; and Welling, M. 2016. Semi-supervised classification with graph convolutional networks. *arXiv preprint arXiv:1609.02907*.
- Kothapalli, V.; Tiner, T.; and Bruna, J. 2024. A neural collapse perspective on feature evolution in graph neural networks. *Advances in Neural Information Processing Systems*, 36.
- Lee, S. Y.; Bu, F.; Yoo, J.; and Shin, K. 2023. Towards deep attention in graph neural networks: Problems and remedies. In *International Conference on Machine Learning*, 18774–18795. PMLR.
- Lei, R.; Wang, Z.; Li, Y.; Ding, B.; and Wei, Z. 2022. EvenNet: Ignoring Odd-Hop Neighbors Improves Robustness of Graph Neural Networks. *arXiv preprint arXiv:2205.13892*.
- Li, B.; Pan, E.; and Kang, Z. 2024. Pc-conv: Unifying homophily and heterophily with two-fold filtering. In *Proceedings of the AAAI Conference on Artificial Intelligence*, volume 38, 13437–13445.
- Li, T. W.; Mei, Q.; and Ma, J. 2024. A metadata-driven approach to understand graph neural networks. *Advances in Neural Information Processing Systems*, 36.
- Li, X.; Zhu, R.; Cheng, Y.; Shan, C.; Luo, S.; Li, D.; and Qian, W. 2022. Finding Global Homophily in Graph Neural Networks When Meeting Heterophily. *arXiv preprint arXiv:2205.07308*.
- Liao, N.; Luo, S.; Li, X.; and Shi, J. 2024. LD2: Scalable Heterophilous Graph Neural Network with Decoupled Embeddings. *Advances in Neural Information Processing Systems*, 36.
- Lim, D.; Hohne, F.; Li, X.; Huang, S. L.; Gupta, V.; Bhalerao, O.; and Lim, S. N. 2021. Large scale learning on non-homophilous graphs: New benchmarks and strong simple methods. *Advances in Neural Information Processing Systems*, 34: 20887–20902.
- Lu, Q.; Zhu, J.; Luan, S.; and Chang, X.-W. 2024. Representation learning on heterophilic graph with directional neighborhood attention. *arXiv preprint arXiv:2403.01475*.
- Luan, S.; Hua, C.; Lu, Q.; Zhu, J.; Zhao, M.; Zhang, S.; Chang, X.-W.; and Precup, D. 2022. Revisiting heterophily for graph neural networks. *arXiv preprint arXiv:2210.07606*.

- Luo, D.; Cheng, W.; Yu, W.; Zong, B.; Ni, J.; Chen, H.; and Zhang, X. 2021. Learning to drop: Robust graph neural network via topological denoising. In *Proceedings of the 14th ACM International Conference on Web Search and Data Mining*, 779–787.
- Ma, Y.; Liu, X.; Shah, N.; and Tang, J. 2021. Is homophily a necessity for graph neural networks? *arXiv preprint arXiv:2106.06134*.
- Mao, H.; Chen, Z.; Jin, W.; Han, H.; Ma, Y.; Zhao, T.; Shah, N.; and Tang, J. 2024. Demystifying structural disparity in graph neural networks: Can one size fit all? *Advances in neural information processing systems*, 36.
- Oono, K.; and Suzuki, T. 2019. Graph neural networks exponentially lose expressive power for node classification. *arXiv preprint arXiv:1905.10947*.
- Pei, H.; Wei, B.; Chang, K. C.-C.; Lei, Y.; and Yang, B. 2020. Geom-gcn: Geometric graph convolutional networks. *arXiv preprint arXiv:2002.05287*.
- Platonov, O.; Kuznedelev, D.; Babenko, A.; and Prokhorenkova, L. 2024. Characterizing graph datasets for node classification: Homophily-heterophily dichotomy and beyond. *Advances in Neural Information Processing Systems*, 36.
- Qiu, C.; Nan, G.; Xiong, T.; Deng, W.; Wang, D.; Teng, Z.; Sun, L.; Cui, Q.; and Tao, X. 2024. Refining Latent Homophilic Structures over Heterophilic Graphs for Robust Graph Convolutional Networks. In *Proceedings of the AAAI Conference on Artificial Intelligence*, volume 38, 8930–8938.
- Rozemberczki, B.; Davies, R.; Sarkar, R.; and Sutton, C. 2019. Gemsec: Graph embedding with self clustering. In *Proceedings of the 2019 IEEE/ACM international conference on advances in social networks analysis and mining*, 65–72.
- Seneta, E. 2006. *Non-negative matrices and Markov chains*. Springer Science & Business Media.
- Tang, B.; Wu, Z.; Wu, X.; Huang, Q.; Chen, J.; Lei, S.; and Meng, H. 2024. SimCalib: Graph Neural Network Calibration Based on Similarity between Nodes. In *Proceedings of the AAAI Conference on Artificial Intelligence*, volume 38, 15267–15275.
- Tang, J.; Sun, J.; Wang, C.; and Yang, Z. 2009. Social influence analysis in large-scale networks. In *Proceedings of the 15th ACM SIGKDD international conference on Knowledge discovery and data mining*, 807–816.
- Tian, Y.; Zhang, C.; Guo, Z.; Zhang, X.; and Chawla, N. 2022. Learning mlps on graphs: A unified view of effectiveness, robustness, and efficiency. In *The Eleventh International Conference on Learning Representations*.
- Velickovic, P.; Cucurull, G.; Casanova, A.; Romero, A.; Lio, P.; and Bengio, Y. 2017. Graph attention networks. *stat*, 1050: 20.
- Wang, T.; Jin, D.; Wang, R.; He, D.; and Huang, Y. 2022. Powerful graph convolutional networks with adaptive propagation mechanism for homophily and heterophily. In *Proceedings of the AAAI Conference on Artificial Intelligence*, volume 36, 4210–4218.
- Wang, X.; and Zhang, M. 2022. How powerful are spectral graph neural networks. In *International Conference on Machine Learning*, 23341–23362. PMLR.
- Wu, X.; Ajorlou, A.; Wu, Z.; and Jadbabaie, A. 2024. Demystifying oversmoothing in attention-based graph neural networks. *Advances in Neural Information Processing Systems*, 36.
- Xu, K.; Li, C.; Tian, Y.; Sonobe, T.; Kawarabayashi, K.-i.; and Jegelka, S. 2018. Representation learning on graphs with jumping knowledge networks. In *International conference on machine learning*, 5453–5462. PMLR.
- Yan, Y.; Chen, Y.; Chen, H.; Xu, M.; Das, M.; Yang, H.; and Tong, H. 2024. From trainable negative depth to edge heterophily in graphs. *Advances in Neural Information Processing Systems*, 36.
- Yan, Y.; Hashemi, M.; Swersky, K.; Yang, Y.; and Koutra, D. 2021. Two sides of the same coin: Heterophily and oversmoothing in graph convolutional neural networks. *arXiv preprint arXiv:2102.06462*.
- Yang, H.; Ma, K.; and Cheng, J. 2021. Rethinking graph regularization for graph neural networks. In *Proceedings of the AAAI Conference on Artificial Intelligence*, volume 35, 4573–4581.
- Zhao, K.; Kang, Q.; Song, Y.; She, R.; Wang, S.; and Tay, W. P. 2023. Graph neural convection-diffusion with heterophily. *arXiv preprint arXiv:2305.16780*.
- Zheng, X.; Zhang, M.; Chen, C.; Zhang, Q.; Zhou, C.; and Pan, S. 2023. Auto-heg: Automated graph neural network on heterophilic graphs. *arXiv preprint arXiv:2302.12357*.
- Zhu, J.; Yan, Y.; Zhao, L.; Heimann, M.; Akoglu, L.; and Koutra, D. 2020. Beyond homophily in graph neural networks: Current limitations and effective designs. *Advances in Neural Information Processing Systems*, 33: 7793–7804.

Technical Appendix

Appendix A (proof of lemma 3 - 5)

In this section, we derive the expected distribution after three types of message-passing (MP) using a multi-class contextual stochastic block model (CSBM), respectively. Before delving into this, let us define these MP schemes again below.

- **Plane MP** inherits the original matrix, which only consists of positive edges.

$$\forall(i, j) \in \mathcal{E}, \tilde{A} = D^{-1}A \geq 0 \quad (31)$$

- **Signed MP** assigns negative values to the heterophilic edges, where $y_i \neq y_j$.

$$\forall(i, j) \in \mathcal{E}, \tilde{A} \in \begin{cases} D^{-1}A, & y_i = y_j \\ -D^{-1}A, & y_i \neq y_j \end{cases} \quad (32)$$

- **Blocked MP** blocks the information propagation for heterophilic edges by assigning zero.

$$\forall (i, j) \in \mathcal{E}, \tilde{A} \in \begin{cases} D^{-1}A, & y_i = y_j \\ 0, & y_i \neq y_j \end{cases} \quad (33)$$

A.1. Proof of Lemma 3 (Plane MP)

Let's assume that $y_i = 0$, ego $k \sim (\mu, \pi/2, 0)$, and aggregated neighbors $k' \sim (\mu, \pi/2, \theta')$. Though each neighbor has multiple distributions proportional to the number of classes, their aggregation always satisfies $|k'| \leq \mu$ since the summation of coefficients $(1 - b_i)$ is lower than 1. Thus, we indicate k'_{aggr} as k' here for brevity. Given this, the expectation after plane MP $\mathbb{E}_p(h_i^{(1)}|y_i, d_i)$ can be retrieved as below:

$$\mathbb{E}_p(h_i^{(1)}|y_i, d_i) = \frac{k}{d_i + 1} + \sum_{j \in \mathcal{N}_i} \left(\frac{k(1-e) + ke}{\sqrt{(d_i+1)(d_j+1)}} b_i + \frac{k'(1-e) + k'e}{\sqrt{(d_i+1)(d_j+1)}} (1-b_i) \right) \quad (34)$$

$$= \frac{k}{d_i + 1} + \sum_{j \in \mathcal{N}_i} \left(\frac{kb_i + k'(1-b_i)}{\sqrt{(d_i+1)(d_j+1)}} \right) \quad (35)$$

$$= \frac{k}{d_i + 1} + \frac{\{kb_i + k'(1-b_i)\}d'_i}{d_i + 1} \quad (36)$$

$$= \frac{\{kb_i + k'(1-b_i)\}d'_i + k}{d_i + 1} \quad (37)$$

$$(38)$$

A.2. Proof of Lemma 4 (Signed MP)

Similar to the above analysis, we can retrieve the expectation $\mathbb{E}_s(h_i^{(1)}|y_i, d_i)$ after signed MP. For this, we employ the edge classification error rate e , which determines the error ratio of finding heterophilic edges as follows:

$$\mathbb{E}_s(h_i^{(1)}|y_i, d_i) = \frac{k}{d_i + 1} + \sum_{j \in \mathcal{N}_i} \left(\frac{k(1-e) - ke}{\sqrt{(d_i+1)(d_j+1)}} b_i + \frac{-k'(1-e) + k'e}{\sqrt{(d_i+1)(d_j+1)}} (1-b_i) \right) \quad (39)$$

$$= \frac{k}{d_i + 1} + \sum_{j \in \mathcal{N}_i} \left(\frac{k(1-2e)b_i - k'(1-2e)(1-b_i)}{\sqrt{(d_i+1)(d_j+1)}} \right) \quad (40)$$

$$= \frac{k}{d_i + 1} + \sum_{j \in \mathcal{N}_i} \left(\frac{(1-2e)\{kb_i + k'(b_i - 1)\}}{\sqrt{(d_i+1)(d_j+1)}} \right) \quad (41)$$

$$= \frac{k}{d_i + 1} + \frac{(1-2e)\{kb_i + k'(b_i - 1)\}d'_i}{d_i + 1} \quad (42)$$

$$= \frac{(1-2e)\{b_i k + (b_i - 1)k'\}d'_i + k}{d_i + 1} \quad (43)$$

A.3. Proof of Lemma 5 (Blocked MP)

Lastly, the expectation $\mathbb{E}_b(h_i^{(1)}|y_i, d_i)$ of assigning zero weights for heterophilic edges is given by:

$$\mathbb{E}_b(h_i^{(1)}|y_i, d_i) = \frac{k}{d_i + 1} + \sum_{j \in \mathcal{N}_i} \left(\frac{k(1-e) - ke \times 0}{\sqrt{(d_i+1)(d_j+1)}} b_i + \frac{-k'(1-e)}{\sqrt{(d_i+1)}} \right) \quad (44)$$

$$= \frac{k}{d_i + 1} + \sum_{j \in \mathcal{N}_i} \left(\frac{k(1-e)b_i + k'e(1-b_i)}{\sqrt{(d_i+1)(d_j+1)}} \right) \quad (45)$$

$$= \frac{k}{d_i + 1} + \frac{\{(1-e)b_i k + e(1-b_i)k'\}d'_i}{d_i + 1} \quad (46)$$

$$= \frac{\{(1-e)b_i k + e(1-b_i)k'\}d'_i + k}{d_i + 1} \quad (47)$$

Appendix B (entropy between signed and blocked MP)

We aim to prove that signed MP introduces higher entropy than the blocked ones. Let us assume an ego i with label k and its neighbor node j is connected to i with a signed edge. Firstly, the true label probability (k) of node b $\hat{y}_{b,k}$ increases, while other probabilities $\hat{y}_{b,o}$ ($o \neq k$) decrease as follows:

$$\hat{y}_p^{(t+1)} \in \begin{cases} \hat{y}_{b,k}^t - \eta \nabla_b \mathcal{L}_{nll}(Y_i, \hat{Y}_i)_k > \hat{y}_{b,k}^t \\ \hat{y}_{b,o}^t - \eta \nabla_b \mathcal{L}_{nll}(Y_i, \hat{Y}_i)_o < \hat{y}_{b,o}^t \quad \forall o \neq k. \end{cases} \quad (48)$$

Now, we analyze the partial derivative $\nabla_b \mathcal{L}_{nll}(Y_i, \hat{Y}_i)_o$ for $\forall o \neq k$,

$$\nabla_b \mathcal{L}_{nll}(Y_i, \hat{Y}_i)_o = \frac{\partial \mathcal{L}_{nll}(Y_i, \hat{Y}_i)_o}{\partial \hat{y}_{b,o}} = \frac{\partial \mathcal{L}_{nll}(Y_i, \hat{Y}_i)_o}{\partial \hat{y}_{i,o}} \cdot \frac{\partial \hat{y}_{i,o}}{\partial \hat{y}_{b,o}^{(L)}} \quad (49)$$

$$= \frac{1}{\hat{y}_{i,o}} \cdot (\hat{y}_{i,o}(1 - \hat{y}_{i,o})) = 1 - \hat{y}_{i,o} > 0, \quad (50)$$

On the contrary, the gradient of node s has a different sign with node p , where we can infer that:

$$\hat{y}_s^{(t+1)} \in \begin{cases} \hat{y}_{s,k}^t - \eta \nabla_s \mathcal{L}_{nll}(Y_i, \hat{Y}_i)_k < \hat{y}_{s,k}^t, \\ \hat{y}_{s,o}^t - \eta \nabla_s \mathcal{L}_{nll}(Y_i, \hat{Y}_i)_o > \hat{y}_{s,o}^t, \quad \forall o \neq k \end{cases} \quad (51)$$

Based on the above analysis, as the training epoch t proceeds, the expectation of signed MP prediction (\hat{y}_s) exhibits higher entropy $H(\mathbb{E}[\hat{y}_s])$ compared to that (\hat{y}_b) of blocked MP $H(\mathbb{E}[\hat{y}_b])$ as below:

$$H(\mathbb{E}[\hat{y}_s^{(t+1)}]) - H(\mathbb{E}[\hat{y}_b^{(t+1)}]) > H(\mathbb{E}[\hat{y}_s^t]) - H(\mathbb{E}[\hat{y}_b^t]). \quad (52)$$

Appendix C (Homophily Estimation)

As defined in Eq. 18, our homophily estimation combines the mechanisms of MLP (Wang et al. 2022) and EvenNet (Lei et al. 2022) as follows:

$$b_i = B_i B_i^T, \dots, B := \sigma \left(\sum_{l=0}^L XW^l + \sum_{l=0}^{\lfloor L/2 \rfloor} \tilde{A}^{2l} XW^l \right) \quad (53)$$

In this equation, the left term $\sum_{l=0}^L XW^l$ employs blocked MP (MLP), while the right term only receives messages from even-hop neighbors (EvenNet). This approach reduces the prediction variance caused by homophily changes while maintaining average performance.

To begin, let us define the k -step homophily ratio \mathbb{H}_k , following (Lei et al. 2022), under *i.i.d.* graphs as follows:

$$\mathbb{H}_k = \frac{1}{N} \sum_{l=0}^{K-1} \left(\Pi_{ll}^k - \sum_{m \neq l} \Pi_{lm}^k \right), \dots, \text{where}, \Pi^k = Y^T \tilde{A}^k Y \quad (54)$$

Since the first term is shared by all k -step propagations, the above equation can be rewritten as:

$$\mathbb{H}_k \approx \sum_{i=0}^k \theta_i \mathbb{H}_i(\Pi) = \theta_0 + \theta_1(I - \tilde{L}) + \dots + \theta_k(I - \tilde{L})^k \quad (55)$$

Combining the notions of MLP and EvenNet, the equation becomes:

$$\mathbb{H}_0 + \mathbb{H}_{2k} \approx \theta_0 + \left(\theta_0 + \theta_2(I - \tilde{L})^2 + \dots + \theta_{2k}(I - \tilde{L})^{2k} \right) \quad (56)$$

By dividing the above equation by 2, we can infer that $\mathbb{E}[\mathbb{H}_0 + \mathbb{H}_{2k}] = \mathbb{E}[\mathbb{H}_{2k}]$, but $\text{Var}[\mathbb{H}_0 + \mathbb{H}_{2k}] < \text{Var}[\mathbb{H}_{2k}]$. This can enhance heterophily robustness (reduced variance) while maintaining overall performance (expectation).

Appendix D (Details of Empirical Analysis)

Figure 1 presents empirical analyses to verify Theorems 10 (left) and 11 (right). For homophily estimation, we use early stopping, saving the predictions with the best validation score if there is no improvement for more than 100 epochs. The edge error estimation follows a slightly different approach, where the (*true*) values are based on the maximum predicted node class as shown below:

$$\forall (i, j) \in \mathcal{E}, \tilde{\mathcal{E}}_{ij}^t \in \begin{cases} 1, & \hat{Y}_i^t = \hat{Y}_j^t \\ 0, & \hat{Y}_i^t \neq \hat{Y}_j^t \end{cases} \quad (57)$$

where \hat{Y}^t stands for the predicted class at step t . The score s can be derived as follows:

$$s = 1 - \frac{1^T \sum_{i=1}^N \sum_{j=1}^N \tilde{\mathcal{E}}_{ij}^t}{|\mathcal{E}|} \quad (58)$$

Conversely, the (*pred*) values are derived through Eq. 19. Additional experimental results are provided in Appendix F.

Appendix E (proof of Theorem 11)

In Theorem 11, we stated that edge error ratio e_t can be inferred using the node classification accuracy of validation sets (α_{t-1}) at iteration $t - 1$ and the number of classes (c). The proof is as follows:

$$e_t = 1 - p(\text{correct edge classification}) \quad (59)$$

$$= 1 - \left\{ \frac{\alpha_{t-1}}{c} * \frac{\alpha_{t-1}}{c} * c^2 + \frac{1 - \alpha_{t-1}}{c - 1} * \frac{1 - \alpha_{t-1}}{c - 1} * (c - 1) \right\} \quad (60)$$

$y_i = y_j$ $y_i \neq y_j$

$$= 1 - \left\{ \alpha_{t-1}^2 + \frac{(1 - \alpha_{t-1})^2}{c - 1} \right\} \quad (61)$$

If two nodes share the same label ($y_i = y_j$), the edge classification accuracy should be proportional to the product of their validation scores. Conversely, if they have different labels, the edge is correctly classified only if both nodes are incorrectly predicted to have the same label.

Appendix F (more experiments about Theorem 10 and 11 under *i.i.d.* graphs)

In addition to Appendix D, we aim to demonstrate that our theorem can estimate the parameters under an *i.i.d.* graph. Following (Kothapalli, Tirer, and Bruna 2024), we construct a graph with $N = 1,000$ nodes, $c = 2$ classes, and $|\mathcal{E}| = 10,000$ edges. For each class, the node features are sampled from a Gaussian distribution. Additionally, we fix the degree of each node as $\mathcal{E}/N = 10$ and set the homophily ratio to match the original data. As shown in Figure 4, the predictions are nearly accurate under this condition, validating our analysis of the two theorems.

Appendix G (Miscellaneous)

This section introduces several details: (1) time complexity of our model, (2) datasets, (3) implementation, and (4) baselines.

G.1. Time Complexity of Calibrated GCN

To begin with, please note that the edge calibration component of our model should be proportional to baseline algorithms such as GPRGNN, FAGCN, or GGCN. Therefore, we focus on the parameter estimation network's complexity, consisting of plain MLP and even-hop propagation networks. Firstly, it is well known that the cost of the MLP follows $\mathcal{O}(nz(X)F' + F'C)$, where $nz(\cdot)$ represents the non-zero elements of the inputs, F' denotes the hidden dimension, and C is the number of classes. The second part involves even-hop message passing (MP), which can be defined as $\mathcal{O}(L|\mathcal{E}|\theta_{GCN}/2)$. In summary, the overall cost should be $\mathcal{O}(nz(X)F' + F'C + L|\mathcal{E}|\theta_{GCN}/2)$, which may require double the computational cost compared to the

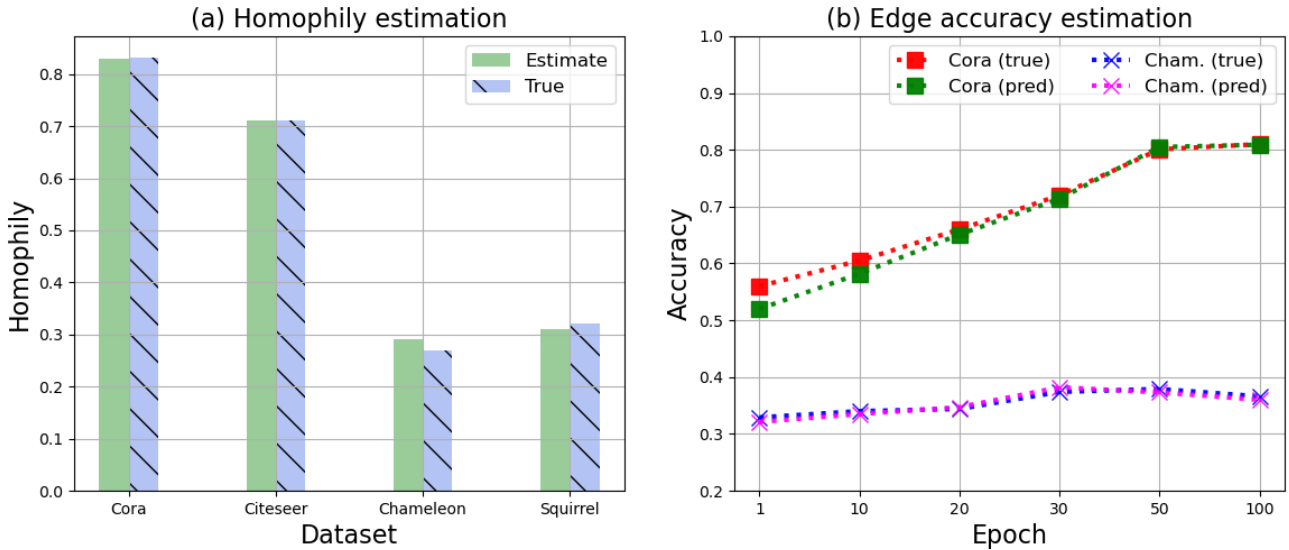


Figure 4: Homophily and edge accuracy (1-error) estimation under *i.i.d.* graphs

baseline methods.

G.2. Datasets

The statistical details of the datasets are in Table 1. (1) *Cora*, *Citeseer*, *Pubmed* (Kipf and Welling 2016) are citation graphs where a node corresponds to a paper, and edges are citations between them. The labels represent the research topics of the papers. (2) *Actor* (Tang et al. 2009) is a co-occurrence graph of actors appearing in the same movie. The labels represent five types of actors. (3) *Chameleon*, *Squirrel* (Rozemberczki et al. 2019) are Wikipedia hyperlink networks. Each node is a webpage, and the edges are hyperlinks. Nodes are categorized into five classes based on monthly traffic.

G.3. Implementation Details

All methods, including baselines and ours, are implemented using *PyTorch Geometric*¹. For a fair comparison, we set the hidden dimension for all methodologies to 64. ReLU with dropout is used for non-linearity and to prevent overfitting. We use log-Softmax as the cross-entropy function. The learning rate is set to $1e^{-3}$, and the Adam optimizer is used with a weight decay of $5e^{-4}$. For training, 20 nodes per class are randomly chosen, and the remaining nodes are divided into two parts for validation and testing, following the settings in (Kipf and Welling 2016).

G.4. Baselines

- **GCN** (Kipf and Welling 2016) is a first-order approximation of Chebyshev polynomials (Defferrard, Bresson, and Vandergheynst 2016). For all datasets, we simply take 2 layers of GCN.
- **APPNP** (Gasteiger et al. 2018) combines personalized PageRank on GCN. We stack 10 layers and set the tele-

port probability (α) as $\{0.1, 0.1, 0.1, 0.5, 0.2, 0.3\}$ for Cora, Citeseer, Pubmed, Actor, Chameleon, and Squirrel.

- **GAT** (Velickovic et al. 2017) calculates feature-based attention for edge coefficients. Similar to GCN, we construct 2 layers of GAT. The pair of (hidden dimension, head) is set as (8, 8) for the first layer, while the second layer is (1, # of classes).
- **GCNII** (Chen et al. 2020) integrates an identity mapping function on APPNP. We set $\alpha = 0.5$ and employ nine hidden layers. We increase the weight of identity mapping (β) that is inversely proportional to the heterophily of the dataset.
- **H₂GCN** (Zhu et al. 2020) suggests the separation of ego and neighbors during aggregation. We refer to the publicly available *source code*² for implementation.
- **PTDNet** (Luo et al. 2021) removes disassortative edges before a message-passing. We also utilize the open *source code*³ and apply confidence calibration.
- **P-reg** (Yang, Ma, and Cheng 2021) ensembles a regularization term to provide additional information that training nodes might not capture. (*source code*⁴)
- **HOG-GCN** (Wang et al. 2022) adaptively controls the propagation mechanism by measuring the homophily degrees between two nodes. (*source code*⁵)
- **JacobiConv** (Wang and Zhang 2022) studies the expressive power of spectral GNN and establishes a connection with the graph isomorphism testing. (*source code*⁶)

²<https://github.com/GemsLab/H2GCN>

³<https://github.com/flyingdoog/PTDNet>

⁴<https://github.com/yang-han/P-reg>

⁵<https://github.com/hedongxiao-tju/HOG-GCN>

⁶<https://github.com/GraphPKU/JacobiConv>

¹<https://pytorch-geometric.readthedocs.io/en/latest/modules/nn.html>

- **GloGNN** (Li et al. 2022) receives information from global nodes, which can accelerate neighborhood aggregation. (*source code*⁷)
- **ACM-GCN** (Luan et al. 2022) suggests a local diversification operation through the adaptive channel mixing algorithm. (*source code*⁸)
- **AERO-GCN** (Lee et al. 2023) improves the deep graph attention to reduce the smoothing effect and improve the performance at deep layers (*source code*⁹).
- **Auto-HeG** (Zheng et al. 2023) automatically build heterophilic GNN models with search space design, super-net training, and architecture selection (*source code*)¹⁰.
- **TED-GCN** (Yan et al. 2024) redefines GCN’s depth L as a trainable parameter, which can control its signal processing capability to model both homophily/heterophily graphs.
- **PCNet** (Li, Pan, and Kang 2024) proposes a two-fold filtering mechanism to extract homophily in heterophilic graphs (*source code*)¹¹.
- **GPRGNN** (Chien et al. 2020) generalized the personalized PageRank to deal with heterophily and over-smoothing. Referring to the open source *code*¹², we tune the hyper-parameters based on the best validation score for each dataset.
- **FAGCN** (Bo et al. 2021) determines the sign of edges using the node features. We implement the algorithm based on the *sources*¹³ and tune the hyper-parameters concerning their accuracy.
- **GGCN** (Yan et al. 2021) proposes the scaling of degrees and the separation of positive/negative adjacency matrices. We simply take the publicly available *code*¹⁴ for evaluation.

⁷<https://github.com/RecklessRonan/GloGNN>

⁸<https://github.com/SitaoLuan/ACM-GNN>

⁹<https://github.com/syleeheat/AERO-GNN>

¹⁰<https://github.com/Amanda-Zheng/Auto-HeG>

¹¹<https://github.com/uestclbh/PC-Conv>

¹²<https://github.com/jianhao2016/GPRGNN>

¹³<https://github.com/bdy9527/FAGCN>

¹⁴https://github.com/Yujun-Yan/Heterophily_and_oversmoothing